Frequency Conversion of Phase-Aberrated Laser Beams for the National Ignition Facility

Ronen Mukamel
Brighton High School
Rochester, NY

Advisor: R. S. Craxton
Senior Scientist
Laboratory for Laser Energetics
University of Rochester

Frequency Conversion of Phase-Aberrated Laser Beams for the National Ignition Facility

Summary

I simulated laser beams at the National Ignition Facility passing through frequency conversion crystals, which convert beams from the infrared to the ultraviolet, and phase plates, which distribute the laser's energy uniformly. I calculated the frequency conversion efficiency for designs where the phase plate precedes the crystals, previously thought to be impractical, and found these designs to be efficient and feasible. This is useful because these designs minimize damage to the optics.

Abstract

The effect of the placement of a direct drive phase plate on the frequency conversion efficiency of a National Ignition Facility (NIF) beam was studied. The frequency conversion efficiency was calculated for two possible positions for a direct drive phase plate, before and after the frequency conversion crystals. The phase aberrations arising from the phase plate resulted in only a small decrease in frequency conversion efficiency at a nominal operating point of 3 GW/cm^2 for three representative smoothing by spectral dispersion scenarios, implying that putting the phase plate before the frequency conversion crystals is a feasible option.

1 Introduction

Inertial confinement fusion (ICF) has the potential to solve the world's energy crisis. In fusion, the nuclei of two reactant atoms are joined forming a product nucleus that has less mass than the combined mass of the reactants. The lost mass is converted into energy which can be used to generate electricity. ICF is a scheme for achieving fusion by applying high temperatures and pressures to small, containable fuel pellets.

The National Ignition Facility (NIF) is currently under construction at Lawrence Livermore National Laboratories and upon completion will be the largest laser system in the world (the NIF will consist of 192 high-energy beams producing a total of 1.8 MJ). Studies of ICF will be conducted at the NIF by bombarding small plastic capsules, a few millimeters in diameter, which contain deuterium and tritium (two isotopes of hydrogen, one of the most abundant elements on Earth) with high-energy laser beams through a scheme called indirect

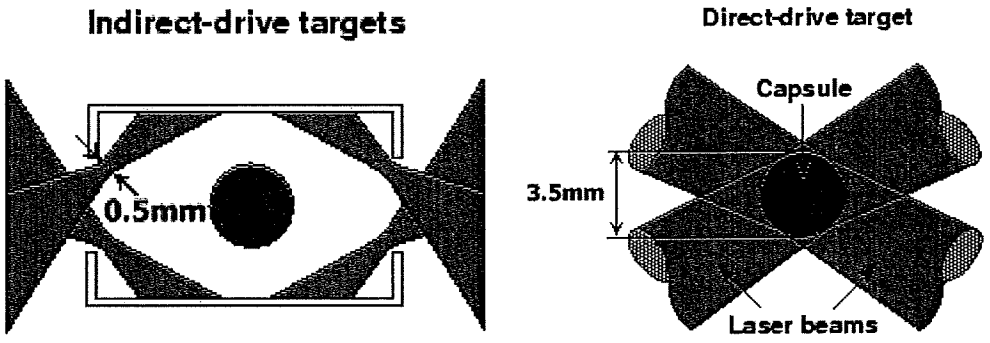

Figure 1: **Indirect and Direct Drive.** Left: Indirect drive involves passing the laser energy into a metallic vessel which absorbs the energy and re-emits it as X-rays which are absorbed by the target. Right: Direct drive is a scheme to achieve ICF by hitting targets with laser energy directly.

drive. Indirect drive involves passing the laser beams into a metallic vessel surrounding the capsule. The walls of the vessel absorb the laser energy and emit X-rays which are absorbed by the capsule.

The Omega laser system, at the University of Rochester's Laboratory for Laser Energetics (LLE), is currently the largest laser system in operation conducting ICF experiments (Omega is a 60-beam system which produces 30 kJ of energy). At Omega, fuels are bombarded through a scheme called direct drive. Each of Omega's laser beams is absorbed by the capsule directly. The two schemes for ICF are depicted in Figure 1. While the NIF is primarily designed for indirect drive experiments, it will be useful to conduct direct drive experiments on the larger system. In direct drive, the laser energy is focused onto the whole target (focal size is 3.5 mm, Figure 1 Right) whereas in indirect drive, the laser energy is focused to fit through a small hole in the metallic vessel (focal size is 0.5 mm, Figure 1 Left). The focus size in direct drive is therefore larger than that in indirect drive. At both systems, the energy absorbed by the capsule causes the outer layer of plastic to ionize, making it a

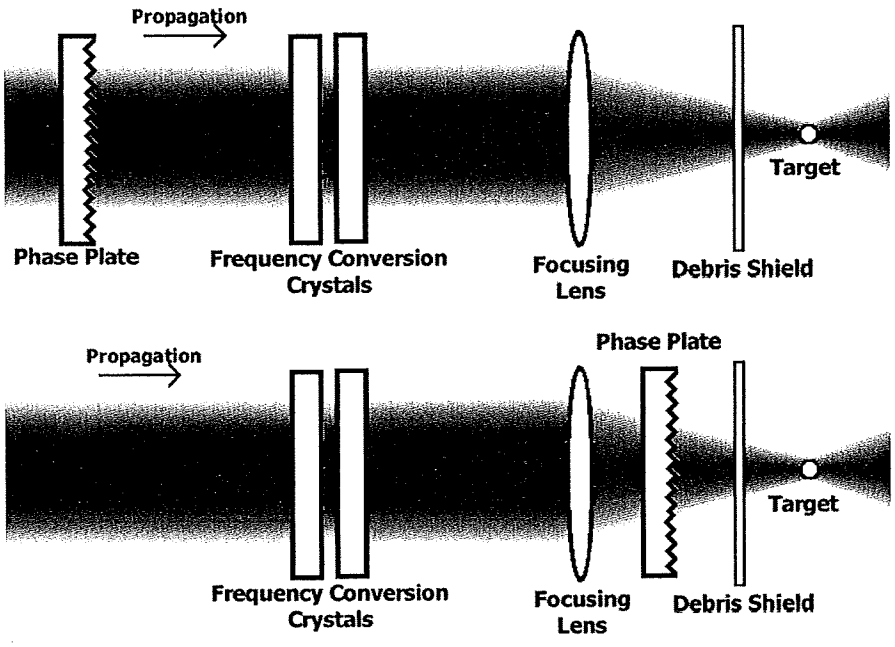

Figure 2: **NIF Final Optics.** Each of NIF's 192 infrared beams is passed through a system of final optics consisting of frequency conversion crystals, a focusing lens, a phase plate and a debris shield. The figure shows two possible placements for the direct drive phase plate.

gas known as plasma. The layer of plasma expands explosively, compressing the rest of the capsule and the fuel, causing the deuterium and tritium to fuse.

At both the NIF and Omega, neodymium:glass beams (beams generated with neodymium-doped glass) with an infrared wavelength of 1.054 μm are frequency converted to ultraviolet beams because infrared beams are not absorbed well. Infrared beams cannot penetrate the layer of plasma surrounding the capsule. Consequently, energy of infrared beams is absorbed by the electrons of the plasma cloud rather than the capsule. These electrons oscillate with the electric field associated with the beams and gain enough kinetic energy to penetrate the plastic capsule and deposit energy in the fuel. The fuel is heated prematurely making it impossible to compress it sufficiently. Higher-frequency ultraviolet beams can penetrate farther into the atmosphere of plasma and are better absorbed [1].

The schematic in Figure 2 (Top) depicts the final optics through which each of the NIF's 192 beams is passed. The beam passes through two frequency conversion crystals which convert the beam's energy from infrared to ultraviolet. The focusing lens focuses the beam's energy on the target. The phase plate is like a piece of frosted glass; the thickness of the phase plate varies from point to point. The phase plate spreads the beam by diffraction, making it phase-aberrated. Beams that are not phase-aberrated are spatially coherent. For indirect drive experiments, this spreading decreases the intensity of the beam which at its focal point (Figure 1 Left) would otherwise overheat the gas in the vessel creating high-energy electrons. These electrons would prematurely heat the fuel in the same manner as the high-energy electrons in the plasma generated by infrared beams heat the fuel. For direct drive experiments, the phase plate serves a different purpose. By spreading energy from each portion of the lens over the whole target, the phase plate eliminates non-uniformities in target irradiation which would lead to uncontrollable implosions (Figure 1 Right). Notice that a phase plate for direct drive experiments would spread the beam with larger angles than a phase plate for indirect drive because the direct drive phase plate must focus the beam onto the whole target whereas the indirect drive phase plate focuses the beam to fit through a small hole in a metallic vessel. Finally, the debris shield prevents debris from the reaction from damaging the final optics.

The arrangement of the final optics for indirect drive experiments at the NIF has the phase plate preceding the frequency conversion crystals (Figure 2 Top). It has already been determined that the small angle deflections created by the indirect drive phase plate will not have a significant impact on frequency conversion efficiency. However, the larger

angle deflections created by the direct drive phase plate could have a significant impact on conversion efficiency if placed before the crystals and it has been believed to date that placing it after the frequency conversion crystals is preferable (Figure 2 Bottom). Placing the phase plate in the ultraviolet portion of the system, however, will limit the intensity allowed through the system because optics in the ultraviolet portion of the system cause self-focusing which can be harmful to the optics (this effect is less significant in the infrared portions of the system).

This investigation analyzes the effect of placing the direct drive phase plate in front of the frequency conversion crystals. Frequency conversion efficiency was calculated for a spatially coherent beam and a beam with phase aberrations due to a phase plate to determine the loss of frequency conversion efficiency in the second final optics design Figure 2 (Bottom). In Section 2, techniques for calculating frequency conversion are discussed. In Section 3, the way the calculation techniques were implemented is described. The results described in Section 4 show that the phase plate for direct drive can be placed before the frequency conversion crystals without suffering a large decrease in conversion efficiency.

2 Simulations of Frequency Conversion

Frequency conversion at the NIF is achieved by passing each of the laser beams through two potassium-dihydrogen phosphate (KDP) crystals (see Figure 3). The doubler crystal converts fundamental Nd:glass infrared beams polarized along the o-axis with wavelength $\lambda = 1.054\ \mu$m to second-harmonic green energy polarized along the e-axis. The tripler combines the green energy and residual infrared energy to form third-harmonic ultraviolet

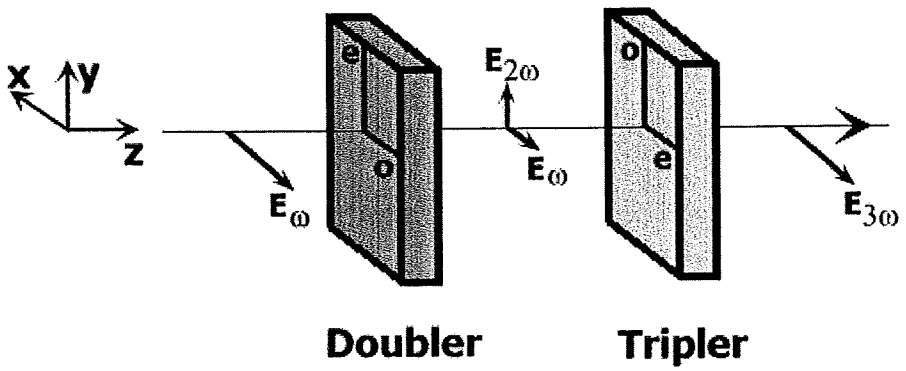

Figure 3: **KDP Crystals.** Each of the NIF's 192 beams is passed through two KDP crystals which convert infrared energy to ultraviolet energy.

energy polarized along the e-axis [2].

In general, an electric field $\mathcal{E}$ associated with a beam of light propagating in the z direction can be represented by the real part of a complex function of time and space:

$$\mathcal{E}(x, y, z, t) = Re\{E(x, y, z, t)e^{i\omega t - ikz}\} \tag{1}$$

Here, E is a complex function of time and space which represents the slowly varying field envelope, ω is the field's frequency, x and y are coordinates perpendicular to the beam direction and the wave-number $k = \omega n/c$ where n is the refractive index and c is the speed of light in a vacuum. The intensity I is proportional to the square of the complex magnitude of E.

When light propagates through a crystal, it induces electronic motion: the associated electric field causes the electrons in the medium to oscillate thereby generating a field of their own which propagates similarly through the crystal. At low field intensities, an electron's oscillation amplitude is linearly proportional to the initial electric field and the electron's

field has the same frequency as the initial electric field. This is known as linear optics. However, two high-intensity fields with frequencies ω and ω' can give rise to oscillating electrons and associated electric fields oscillating at the sum of their frequencies $\omega+\omega'$. This phenomenon is known as sum-frequency generation [3] and is non-linear optics because the resulting field is non-linearly proportional to the initial field. In particular, sum-frequency generation can occur with one intense field whereby $\omega = \omega'$ and $\omega+\omega' = 2\omega$. This is known as second-harmonic generation.

Sum-frequency generation is significant when the generated field propagates at the same speed as the initial field and the electrons in both fields oscillate in phase throughout the sample. This is called phase matching. KDP crystalline structure causes light polarized along the ordinary o-axis to travel with an index of refraction that is independent of the direction of propagation. Light polarized along the extraordinary e-axis travels with an index of refraction that depends upon the direction of propagation. The frequency doubler in Figure 3 is cut at an angle where the speeds of the fundamental and second-harmonic fields are equal.

The growth of the second-harmonic field $E_{2\omega}$ from the initial first-harmonic electric field E_ω as it propagates along an axis z can be described by simultaneous differential equations:

$$\frac{\partial E_\omega}{\partial z} = -i\chi_1 E_{2\omega} E_\omega^* e^{-i\Delta K z} \tag{2a}$$

$$\frac{\partial E_{2\omega}}{\partial z} = -i\chi_2 E_\omega E_\omega e^{i\Delta K z} \tag{2b}$$

Here, E_ω and $E_{2\omega}$ are the slowly varying field envelopes which appear as E in Eq. 1, χ_i are constants (susceptibilities) which describe the tendency of electrons to oscillate with

frequencies ω and 2ω and are determined by properties of the crystal and the way they were cut, and ΔK is the phase matching coefficient which is a function of wavelength and direction of propagation. Eq. 2a describes the first-harmonic field's loss of energy and Eq. 2b describes the generation of the second-harmonic field in accordance with the law of conservation of energy.

Similarly, the tripler crystal in Figure 3 is cut at the angle such that the field emerging from the doubler is phase matched with the third-harmonic field with frequency 3ω polarized along the e-axis. As the field propagates through the tripler, a non-linear field with frequency 3ω is generated by the residual first-harmonic field and the generated second-harmonic field through sum-frequency generation. The generation of a third-harmonic field $E_{3\omega}$ can also be described by differential equations:

$$\frac{\partial E_\omega}{\partial z} = -i\chi_1 E_{3\omega} E^*_{2\omega} e^{-i\Delta K z} \tag{3a}$$

$$\frac{\partial E_{2\omega}}{\partial z} = -i\chi_2 E_{3\omega} E^*_{\omega} e^{-i\Delta K z} \tag{3b}$$

$$\frac{\partial E_{3\omega}}{\partial z} = -i\chi_3 E_{\omega} E_{2\omega} e^{i\Delta K z} \tag{3c}$$

Here, all the terms represent the same quantities as the terms in Eqs. 2.

For both the doubler and tripler crystals, the phase matching coefficient $\Delta K = 0$ in Eqs. 2 and 3 when the crystals are tuned for optimal second-harmonic generation and third-harmonic generation respectively. When ΔK is not 0, the added phase is destructive to frequency conversion. However, since ΔK varies with frequency and deflection angle, ΔK is only 0 when the crystal is tuned for a specific wavelength and angle of propagation. For

example, on a NIF tripler [4], in mks units:

$$\Delta K = \Delta\Theta \cdot (-4.581 \times 10^5) + \Delta\lambda \cdot (-62.7 \times 10^{10}) \tag{4}$$

Here $\Delta\Theta$ is the angle with which the beam is detuned and $\Delta\lambda$ is the frequency shift (from the reference $\lambda = 1.054$ μm). The dependence of ΔK on angle deflections is the source of frequency conversion efficiency losses due to the phase plate. Since the phase plate for direct drive produces larger angle deflections than the phase plate for indirect drive, the phase plate for direct drive would have a larger impact on frequency conversion efficiency.

When the doubler is tuned for optimal second-harmonic generation, almost all of the initial energy is converted to second-harmonic energy and little third-harmonic generation occurs because there are no residual first-harmonic photons to combine with the second-harmonic photons. The doubler is therefore detuned at an angle $\Delta\Theta_d = 350$ μrad so that the field emerging from the doubler contains first-harmonic and second-harmonic photons in the ratio of 1:1 which is optimal for third-harmonic generation.

Wavelength shifts $\Delta\lambda$ affecting ΔK in Eq. 4 are mainly due to a system aimed at achieving better target irradiation uniformity called smoothing by spectral dispersion (SSD) [5, 6]. The phase plates for both direct and indirect drive cause the laser beam to interact with itself, creating an interference pattern at the target. A monochromatic beam passing through the phase plate would create a static interference pattern causing target irradiation nonuniformities. SSD is a system whereby the beam is given bandwidth; the beam's frequency oscillates as a function of space and time. An SSD modulated beam passing through the phase plate generates an interference pattern which averages out over time and uniformly

distributes energy across the target. Since ΔK depends on the wavelength shift, SSD wavelength shifts are destructive to the frequency conversion process. The SSD bandwidth at Omega and NIF is therefore limited. It was originally hypothesized by Eimerl that a larger SSD bandwidth could be frequency converted efficiently if a second tripler, tuned for a different frequency of light, were added [7]. His hypothesis was later verified for the Omega system by Oskoui who showed that three times the SSD bandwidth can be frequency converted with two frequency-tripler crystals tuned for slightly different wavelengths [8]. Eimerl's concept was first demonstrated experimentally by Babushkin, et al. [9]. Recently, a second tripler, tuned according to Oskoui's predictions, was installed on each of Omega's 60 beams.

To describe the SSD profile of the beam, the field envelope E from Eq. 1 is multiplied by an SSD phase term. The final expression for the initial field at $z = 0$ found in the frequency conversion Eqs. 2 and 3 is:

$$E(x, y, 0, t) = \bar{E}(x, y, 0, t) * \exp\{i(\delta_1 sin(\omega_1 t + \alpha_x x + \Phi_x) + \delta_2 sin(\omega_2 t + \alpha_y y + \Phi_y))\} \quad (5)$$

The instantaneous SSD wavelength shift ($\Delta\lambda$), which is used to calculate ΔK from Eq. 4, is given by the t-derivative of the phase exponent:

$$\Delta\lambda(t, x, y) = \Delta\lambda_1 cos(\omega_1 t + \alpha_x x + \Phi_x) + \Delta\lambda_2 cos(\omega_2 t + \alpha_y y + \Phi_y) \quad (6)$$

$$\text{where} \quad \Delta\lambda_1 = -\frac{\lambda^2}{2\pi c}\omega_1\delta_1 \quad \text{and} \quad \Delta\lambda_2 = -\frac{\lambda^2}{2\pi c}\omega_2\delta_2$$

Here $\bar{E}(x, y, 0, t)$ is the real function which represents the spatial and temporal shapes of the laser beam, δ_1 and δ_2 are modulation depths for both dimensions of SSD, ω_1 and ω_2 are SSD

modulation frequencies for the two dimensions of SSD, α_x and α_y are modulation terms for SSD in space, Φ_x and Φ_y are relative phase terms for the two dimensions of SSD, c is the speed of light in a vacuum, and $\lambda = 1.054$ μm is the reference wavelength of the incoming field. The SSD scenarios in calculations about the NIF were based on current SSD designs for Omega because no there is no alternative design for the NIF. For a 1-THz SSD beam, $\Delta\lambda_1 = 5.5$ Å, $\Delta\lambda_2 = 0.75$ Å, $\omega_1 = 2\pi \times 10.5 \times 10^9$Hz, $\omega_2 = 2\pi \times 3.3 \times 10^9$Hz, $\alpha_x = 42.9\text{m}^{-1}$, and $\alpha_y = 23.4\text{m}^{-1}$.

3 Modeling NIF Beams

A code (SPAN, Simulations of Phase-Aberrated NIF beams) was written in PV-WAVE [10], a command-line language, to integrate Eqs. 2 and Eqs. 3 with respect to z to calculate the field emerging from the frequency conversion crystals. The beam is represented by a three-dimensional grid in x, y, and t. Each of the $N_x \times N_y \times N_t$ points in the beam (where N_x, N_y and N_t are the number of pixels in x, y, and t respectively) has three associated quantities: a complex number which represents the electric field at that point (Eq. 1), a wavelength shift due to SSD ($\Delta\lambda$ from Eq. 6) and a deflection angle. Frequency conversion was calculated by integrating Eqs. 2 and 3 for every point in the beam with respect to z according to current specifications for the NIF final optics using the half-step whole-step method of integration. Frequency conversion efficiency Eff for a single point in the beam is the ratio of the final third-harmonic to the initial fundamental intensities:

$$\text{Eff} = \frac{I_{3\omega}}{I_\omega} = \frac{|E_{3\omega}|^2}{|E_\omega|^2} \tag{7}$$

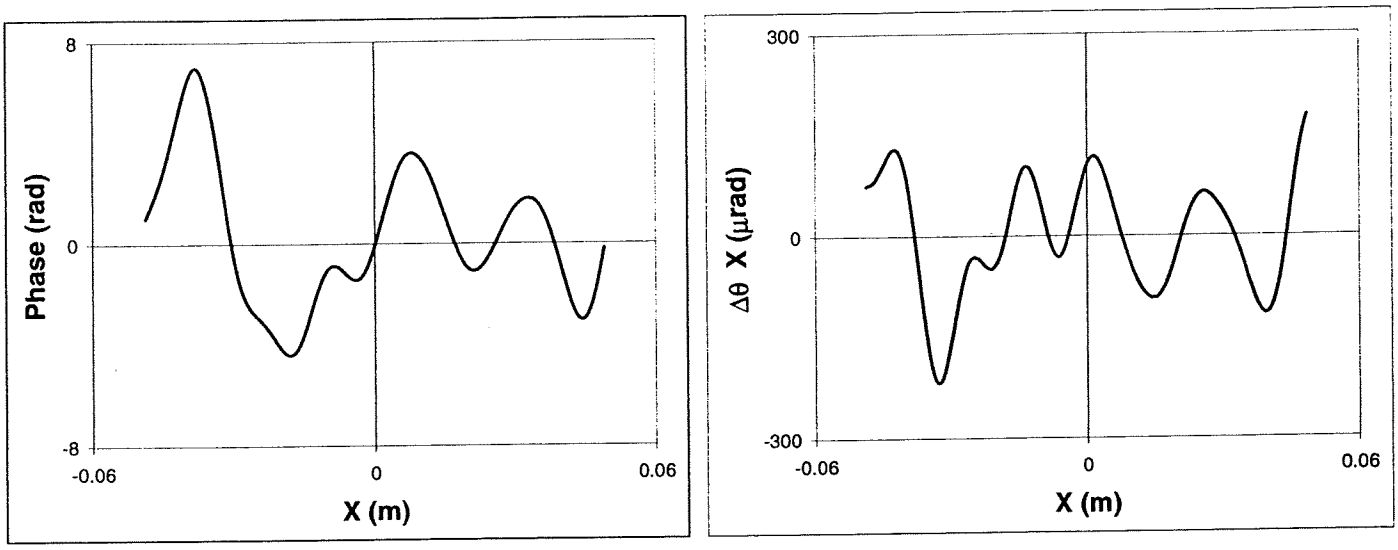

Figure 4: **Direct Drive Phase Plate.** Left: A cross-section of the phase-profile Φ is shown for a direct drive phase plate on the NIF. Right: The angle deflection along the x-axis is calculated from the phase-profile using Eqs. 8.

Here, I_ω and $I_{3\omega}$ are the intensities of the first and third harmonic fields respectively. Frequency conversion for the whole beam is the average efficiency for all points in the beam.

For phase-aberrated beams, each point in the beam is given an angle shift in x and y, which is calculated from an input phase profile of the phase-aberrated beam. The phase profile was scaled from a 27 cm beam diameter Omega direct drive phase plate designed by Lin et al. [11] to the 35 cm diameter of the NIF beam because no alternative design for the NIF has been proposed. The phase profile was also scaled so that the associated angle deflections produced a target irradiation profile that is consistent with current designs which are gaussian with the e^{-1} point 1112 μm from the maximum [12]. In Figure 4, the phase profile Φ of the beam emerging from the direct drive phase plate scaled to the NIF is shown for a portion of the beam about 10 cm along the x-axis (Left). The angle deflections due to

the phase plate are calculated from the phase profile:

$$\begin{aligned} \Delta\Theta_x(x,y) &= \arctan \tfrac{\partial\Phi(x,y)}{\partial x}/k \\ \Delta\Theta_y(x,y) &= \arctan \tfrac{\partial\Phi(x,y)}{\partial y}/k \end{aligned} \tag{8}$$

Here, $\Delta\Theta_x$ and $\Delta\Theta_y$ are the angle deflections along the x and y-axes respectively and are functions of x and y and k is the wave-number which appears in Eq. 1. In Figure 4 (Right), the angle deflection calculated by SPAN along the x-axis is shown for the same 10 cm portion of the beam.

SPAN was based on an earlier code written by Oskoui [8] and later modified by Grossman [13]. The previous code was written to calculate frequency conversion for a spatially coherent Omega laser beam and had limitations. Since only coherent beams were considered, the previous code considered the beam in the z and t dimensions only and could not calculate frequency conversion efficiency for a phase-aberrated beam. In addition, the SSD profile of the beam was simplified in the code because variations of the SSD profile in x and y (Eq. 5) could not be considered. Also, the previous code could only calculate frequency conversion according to the Omega final optics design which involves a different method of frequency doubling.

4 Results

To verify the accuracy of SPAN in calculating frequency conversion for the NIF final optics design, it was compared with a previous calculation made by Craxton of conversion efficiency

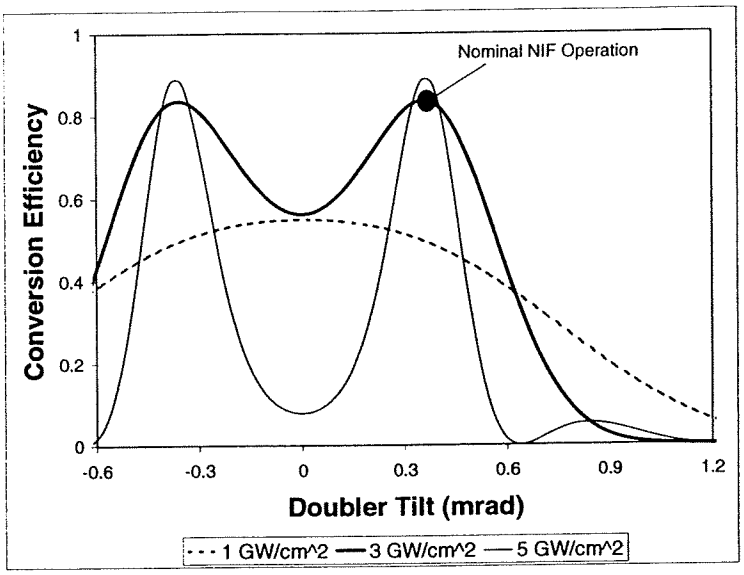

Figure 5: **Verifying NIF Conversion Calculation.** The extended code was used to reproduce the relationship between conversion efficiency and doubler tilt. The NIF nominally operates at 3 GW/cm^2 and $\Delta\Theta_d = 350$ μrad.

for a spatially coherent NIF beam as a function of doubler tilt $\Delta\Theta_d$ [14]. The previous results are reproduced in Figure 5.

The shape of the third harmonic conversion with respect to doubler tilt (for the 3 GW/cm^2 case, the thick solid line) illustrates an important property of the NIF final optics design. The curve has a minimum at $\Delta\Theta_d = 0$ μrad which is where the doubler is phase matched and $\Delta K = 0$. Second harmonic conversion efficiency is high and there is little left-over first harmonic energy. When the beam passes through the frequency triplers, there are not enough residual first-harmonic photons to combine with the second-harmonic photons and there is little third harmonic conversion. The doubler is detuned to the nominal operating point of 350 μrad so that second harmonic conversion is exactly 67% and there is one infrared photon left for every green photon generated. This corresponds to a maximum in Figure 5.

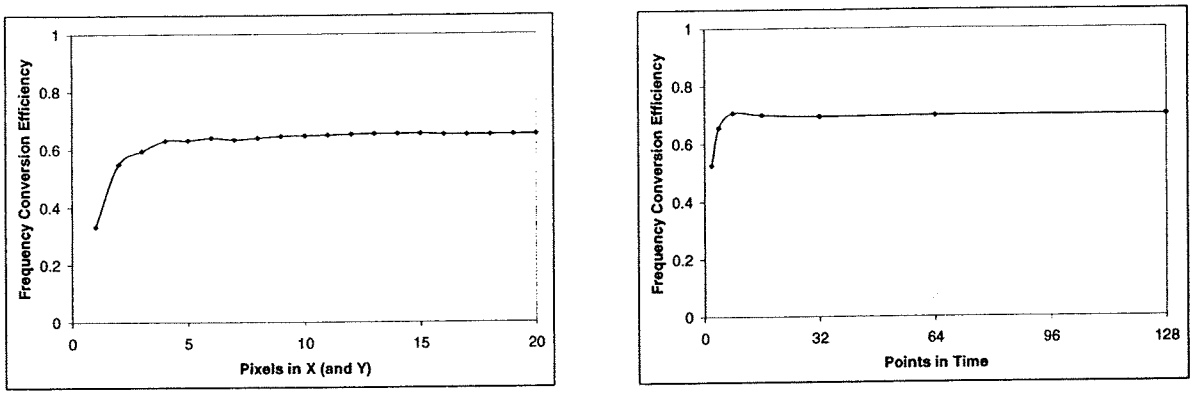

Figure 6: **Convergence of Conversion Efficiency** Left: The conversion efficiency for a 0.5 THz SSD field with $N_x \times N_x \times 50$ pixels is plotted with respect to N_x. Right: Frequency conversion efficiency for a 0.5 THz SSD field with $20 \times 20 \times N_t$ pixels is plotted with respect to N_t.

Three models for SSD were considered. For each SSD set up, conversion efficiency was calculated with the phase plate before and after the frequency conversion crystals. For the first two SSD models, a beam without SSD (0-THz) and a beam with SSD bandwidth of 0.5-THz, the NIF final optics design with one doubler crystal and one tripler crystal was used. If a third crystal were added, extra bandwidth could be passed through the system. The third scenario involved a full 1-THz SSD beam with three frequency conversion crystals.

The dimensions of the portion of the initial beam modeled (in x, y and t) were chosen to ensure convergence of the conversion efficiency. Figure 6 shows the relationship between the frequency conversion efficiency and the number of pixels. On the left, the efficiency is plotted with respect to the number of pixels N_x in the x and y dimensions for the 0.5 THz SSD model where $N_x = N_y$. On the right, the frequency conversion efficiency for the 0.5 THz SSD model is plotted with respect to the number of points in time N_t. The number of steps in z, N_z, was 200 points in each crystal for all scenarios. Grossman used the same

SSD Set-Up	Max SSD $\Delta\lambda$ (Both Dimensions 1 and 2)	Efficiency without Phase Plate	Efficiency with Phase Plate
0 THz Case	$\Delta\lambda_1 = 0.05$Å, $\Delta\lambda_2 = 0.075$Å	83.6%	77.5%
0.5 THz Case	$\Delta\lambda_1 = 2.5$Å, $\Delta\lambda_2 = 0.75$Å	69.9%	64.8%
1 THz Case	$\Delta\lambda_1 = 5.5$Å, $\Delta\lambda_2 = 075$Å	72.5%	67.7%

Table 1: Third-Harmonic Conversion Efficiencies for Various SSD-Setups at the NIF

N_z [13]. The number of points was sufficient to produce accuracy to within $\pm 2\%$ measured by calculating the difference between the beam size considered and a beam half the size considered. The beam dimensions were chosen in the same manner for the other SSD cases.

The actual field dimensions depended upon the SSD model and whether the phase plate was used. Without a phase plate, the beam varies only with time (spatial variations of the beam due to SSD are negligible when considering frequency conversion efficiency) so the dimensions in x and y are both 1. With a phase plate, the beam has an angle spread as a function of x and y. For the 0-THz case, only 1 point in time needs to be considered because the beam does not vary with time. An initial beam that was $80 \times 80 \times 1$ pixels (approximately 12.2cm $\times$ 12.2cm $\times$ 2ns) in x, y, and t respectively was taken with the phase plate. Without the phase plate, the beam size was $1 \times 1 \times 1$ pixels. For the 0.5-THz and the 1-THz cases with the phase plate, a beam with dimensions $20 \times 20 \times 50$ in pixels (approximately 11.5cm $\times$ 11.5cm $\times$ 2ns) in x, y, and t respectively was sufficient to reach a convergent efficiency. Without the phase plate, the beam size was $1 \times 1 \times 50$.

The results of the simulations of conversion efficiency are summarized in Table 1. The direct drive phase plate decreased the conversion efficiency of the NIF beam for the 0-THz, the 0.5-THz and the 1-THz case from 83.6% to 77.5%, from 69.9% to 64.8% and from 72.5%

to 67.7%, respectively. Only a small loss of $< 6\%$ on conversion efficiency arises from phase aberrations due to a direct drive phase plate.

5 Conclusions

Frequency conversion efficiency was calculated for both a spatially coherent NIF beam and a beam with phase aberrations due to a direct drive phase plate. The added phase aberrations resulted in only a small loss ($< 6\%$) in conversion efficiency. Placing the phase plate in front of the frequency conversion crystals could therefore be a viable alternative to the original concept of placing the phase plate after the crystals which would limit the intensity allowed through the system. Further studies should look at the tradeoff between conversion and ultraviolet damage limitations.

6 Acknowledgments

This study would not have been possible without Dr. R. S. Craxton, my advisor. I would also like to thank all of the scientists at the Laboratory for Laser Energetics at the University of Rochester who helped me complete my research. Specifically, I thank Dr. J. Morozas for information about the direct drive phase plate and his help in the calculations.

References

[1] R. S. Craxton, et al. *Progress in Laser Fusion*, **Scientific American** Vol. 255, pg. 68 (1986)

[2] R. S. Craxton. *High Efficiency Frequency Tripling Schemes for High-Power Nd:Glass Lasers*, **IEEE Journal of Quantum Electronics**. Vol. QE-17, pg. 1771 (1981)

[3] N. Bloombergen. *Nonlinear Optics*. Benjamin, New York: 1965.

[4] R. S. Craxton, et al. *Basic Properties of KDP Related to the Frequency Conversion of a 1 μm Laser Radiation*, **IEEE Journal of Quantum Electronics** Vol. QE-17, 1782 (1981)

[5] S. Skupsky & R. S. Craxton. *Irradiation Uniformity for High-Compression Laser-Fusion Experiments*, **Physics of Plasmas** Vol. 6, pg. 2157 (1999)

[6] S. Skupsky, et al. *Improved Laser-Beam Uniformity Using the Angular Dispersion of Frequency-Modulated Light*, **Journal of Applied Physics** Vol. 66, pg. 3456 (1989)

[7] D. Eimerl, et al. *Multicrystal designs for efficient third-harmonic generation*, **Optics Letters** Vol. 22, pg. 1208 (1997)

[8] S. Oskoui. *Broad-Bandwidth Frequency Conversion in Laser Fusion*, **Project report, 1996 Summer Research Program for High School Juniors at the University of Rochester's Laboratory for Laser Energetics** (1996)

[9] A. Babushkin, et al. *Demonstration of dual-tripler, broadband third-harmonic generation and implications for OMEGA and the NIF*, **Reprinted from: Third International Conference on Solid State Lasers for Applciation to Inertial Confinement Fusion** pg. 406 (1998)

[10] *Available from Precision Visuals: Houston, Texas*

[11] Y. Lin, et al. *Design for continuous surface-relief phase plates by surface-based simulated annealing to achieve control of focal-plane irradiance.* **Optics Letters**. Vol. 21, pg. 1703 (1996)

[12] *Data on NIF target specifications were obtained through private communication with R. Town*

[13] P. Grossman. *Group Velocity Effects in Broadband Frequency Conversion on OMEGA*, **Project report, 1998 Summer Research Program for High School Juniors at the University of Rochester's Laboratory for Laser Energetics** (1998)

[14] *Data from previous calculations of the effect of doubler tilt on frequency conversion efficiency was obtained through private communication with R. S. Craxton*